Nanopore Characteristics of Barakar Formation Shales and Their Impact on the Gas Storage Potential of Korba and Raniganj Basins in India

Kumar, Shubham; Chandra, Debanjan; Hazra, Bodhisatwa; Vishal, Vikram; Pathegama Gamage, Ranjith

DOI
10.1021/acs.energyfuels.3c03374

Publication date
2024

Document Version
Final published version

Published in
Energy and Fuels

Citation (APA)
Kumar, S., Chandra, D., Hazra, B., Vishal, V., & Pathegama Gamage, R. (2024). Nanopore Characteristics of Barakar Formation Shales and Their Impact on the Gas Storage Potential of Korba and Raniganj Basins in India. *Energy and Fuels*, *38*(5), 3833-3847. https://doi.org/10.1021/acs.energyfuels.3c03374

energy&fuels

pubs.acs.org/EF

Article

Nanopore Characteristics of Barakar Formation Shales and Their Impact on the Gas Storage Potential of Korba and Raniganj Basins in India

Shubham Kumar, Debanjan Chandra, Bodhisatwa Hazra, Vikram Vishal,* and Ranjith Pathegama Gamage

Cite This: *Energy Fuels* 2024, 38, 3833−3847

Read Online

ACCESS | Metrics & More | Article Recommendations | Supporting Information

ABSTRACT: Lithologically diverse shales were collected from two different proliferous basins, namely, the Korba (SM) and Raniganj Basin (BK) in India, and were experimented with at an isothermal condition using CO_2 and N_2 as probe gases in the low-pressure gas adsorption method, demonstrating the disparity between shale pore attributes and surface roughness. The Korba Basin is one of the potential sites for gas storage and production in India and needs to be explored in terms of pore statistics. Literature reviews demonstrate that pore characteristics in shale changes with depth, organic matter, and mineral composition, which can elucidate the gas storage potential for anthropogenic CO_2 storage. Gas adsorption capacity and surface roughness are directly associated with the difference in organic and mineral compositions, which certainly affects the phase distribution of flow regimes in shale reservoirs. The result determines that micropore and mesopore attributes are in good correlation with the TOC and clay minerals, respectively. SM shale shows 30−37% higher micropore attributes and 17−19% lower mesopore attributes than those of BK shales. Furthermore, the siderite content shows a variance in the pore size distribution in BK shales. The fractal dimension (D_s) is evaluated based on the N_2 adsorption isotherm curve using the Frenkel−Halsey−Hill model. SM shales show a strong correlation with both micropores and mesopores at low relative pressure regimes, while BK shales depict their dominance with mesopores at the high relative pressure regime. Therefore, this research provides a preliminary attempt to determine the influence of changes in the depth, surface roughness, and organic and mineral compositions on shales. However, a complete extrapolation of other reservoir factors, viz., seam thickness, shale−water interaction, and permeability variation at reservoir conditions, is vital to unlocking the technical and environmental feasibility of CO_2 storage and gas production in these basins.

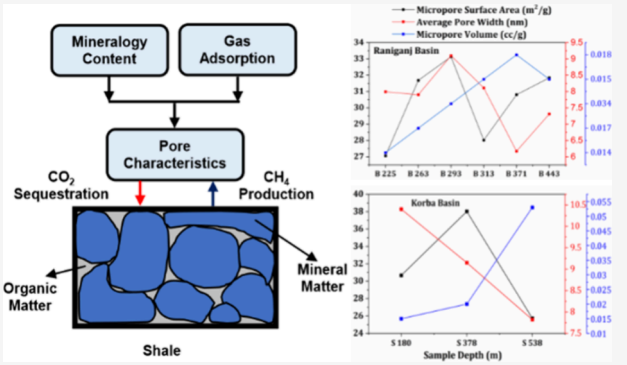

1. INTRODUCTION

Global energy demands are witnessing an outlook for sustainable energy sources and concerns over climate change mitigation. Climate change has drawn the attention of scientists and researchers to unconventional resources, viz., coal bed methane (CBM)[1−4] and shale gas.[5−8] In the past few decades, shale has gained widespread popularity in the USA, Canada, and China as an alternative energy resource to conventional fossil fuels.[9] Shale is a fine-grained complex sedimentary rock that consists of different minerals (viz., quartz, muscovite, clays, carbonates, and feldspar) and organic matter, which influence the gas storage and production.[10−14] Shale acts as a source rock in which the organic matter breaks down into methane-rich gas, primarily due to the thermogenic activities and the occasional biogenic activities in subsurface formations. It also acts as a reservoir rock that is suitable for storage of anthropogenic CO_2. Interpreting pores of shale reservoirs has always been challenging due to the pore framework complexity, which is limited to sophisticated techniques proficient in probing and reconciling the nanoscale pore spectra. The gas storage potential in shale reservoirs is substantially affected by the compositional and structural traits.[15] The shale pore matrix network not only affects the gas sorption capacity but also hydrocarbon (HC) transportation in the shale gas reservoirs. The International Union of Pure and Applied Chemistry (IUPAC) has distinguished the shale pores into various sizes of spectra, namely, macro- (>50 nm), meso- (2−50 nm), and micropores (<2 nm).[16] Gases in shale reservoirs are predominantly adsorbed to the pore walls of micropore sites in organic matter[17−22] and at the surface of clay minerals.[23,24] Gas

Received: September 7, 2023
Revised: February 4, 2024
Accepted: February 5, 2024
Published: February 22, 2024

https://doi.org/10.1021/acs.energyfuels.3c03374
Energy Fuels 2024, 38, 3833−3847

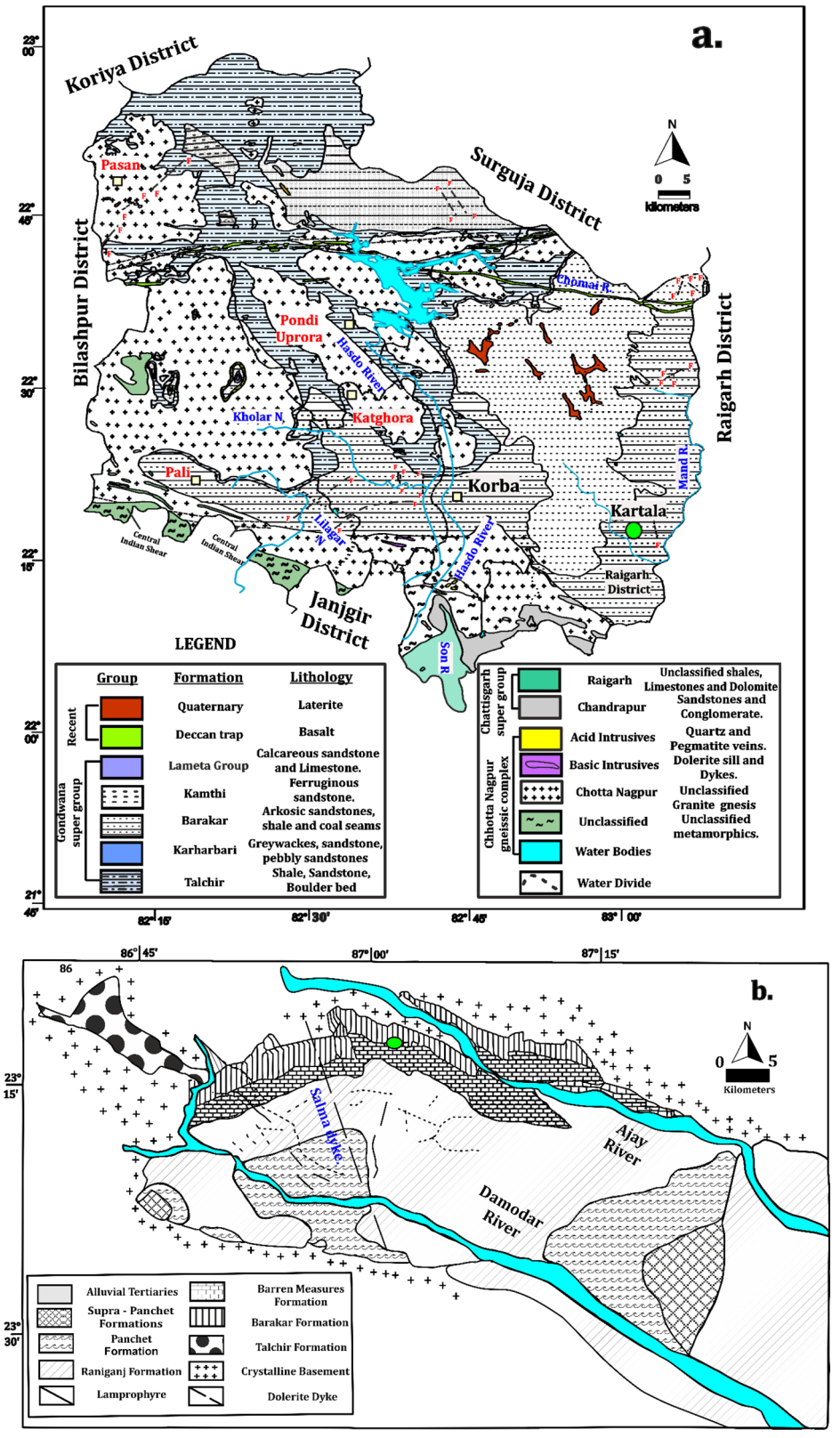

Figure 1. Stratigraphy map of (a) Korba Basin (reproduced with permission from Geological Survey of India.[73] Copyright 2005 Government of India), and (b) Raniganj Basin (reproduced with permission from Chandra et al.[63] Copyright 2020 Elsevier), indicating different study locations and formations. The study locations are marked as green dots.

adsorption in shales is critical to understand for its storage, where the process ranges from 20 to 80%,[18] while gas desorption plays an important role in the long-run gas exploitation. Literature reviews depict that the organic content has a considerable role in gas storage and production since it contributes to the large internal surface area in shales.[25] The organic composition in shales varies from 1 to 20%, which is a key factor responsible for in situ gas storage and generation.

https://doi.org/10.1021/acs.energyfuels.3c03374
Energy Fuels 2024, 38, 3833−3847

Table 1. Mineral Composition for Korba and Raniganj Basin Shales[a]

			clay minerals				
sample name	depth (m)	quartz	kaolinite	illite	feldspar (orthoclase)	muscovite	siderite
SM 1	180	22.1	48.9	0	14.4	14.6	0
SM 2	378	33.4	57.1	0	0	6.6	2.9
SM 3	538	24	50.3	12.9	12.8	0	0
BK 1	225	18.63	46.41	13.11	0	8.53	13.32
BK 2	263	14.54	50.61	24.75	0	0	10.10
BK 3	293	22.73	44.62	19.71	0	8.22	4.72
BK 4	313	19.25	42.68	21.03	0	7.11	9.94
BK 5	371	24.95	20.19	39.09	0	14.25	1.51
BK 6	443	19.79	25.10	25.00	0	24.27	5.83

[a]All values are in wt %.

Thermal maturity, mineral matter, kerogen types, and total organic carbon (TOC) are the prominent parameters responsible for gas production and storage in shale reservoirs.[26−34] Zhang et al. stated that adsorption is an important prospect for gas sorption in both organic matter and clay minerals. Moreover, the authors also reveal a linear relationship between the Brunauer−Emmett−Teller (BET) surface area and methane sorption potential, irrespective of their composition.[25] The clay mineral structure has a crucial role in gas adsorption, and the clay mineral type influences the amount of gases that can be adsorbed.[35] Clay minerals, viz., montmorillonite, illite, smectite, and kaolinite, show a significant influence on the gas storage and transport dynamics.[12,28,36] Literature reviews illustrate that kaolinite and illite have a substantial correlation with the mesopore attributes.[12,29,32,37,38] Various quantitative methods such as low-pressure gas adsorption (LPGA),[34,39−44] mercury intrusion,[11,45] and X-ray and neutron scattering[46−53] techniques have been broadly studied to illustrate the pore accessibility in shales. The pore characterization in the Korba Basin has not been explored earlier, while similar research had been executed by Bhapkar et al.[54] and Hazra et al.[55] in different basins in India.

Initially, Mandelbrot et al. introduced the theory of the fractal dimension (D_s) in porous media to determine the surface pore irregularity and surface roughness.[56] Surface roughness in shales is determined using N_2 adsorption isotherm curves.[11,22,39,57−63] The fractal dimension (D_s) for any surface ranges from 2 to 3, where D_s = 2 and 3 represent the smoothest and roughest surfaces, respectively. Pore surface roughness affects the oil/gas flows in shale reservoirs, which emphasizes the importance of the fractal dimension in shale pore characterization. Based on adsorption isotherms, fractal models such as the analytical model Frenkel−Halsey−Hill (FHH) equations[64−68] have been introduced to explore the surface irregularity of the solid surface. In this study, we aim to understand the disparity between shale pore characteristics, viz., the specific surface area (SSA), pore dimensions, pore size distribution (PSD), and fractal dimension (D_s) of shales collected from two different gas-rich basins, namely, Korba and Raniganj Basins in India. The variation in the pore attributes with changes in TOC, clay mineral composition, and fractal dimension is investigated.

2. SAMPLE DETAILS AND METHODOLOGIES

2.1. Details of the Sample Location. Shales were collected from the Korba Basin (SM) in Chhattisgarh and the Raniganj Basin (BK) in West Bengal, which are situated in the eastern and central parts of India, respectively, as represented by the stratigraphy map in Figure 1. These basins belong to the Gondwana Supergroup. Korba shales were collected from the Kartala block in the south-central part of the Son-Mahanadi River, which has an area of 530 km^2 and comprises latitudes from 22°01′ to 23°01′ N and longitudes from 82°01′ to 83°07′ E. The Korba Basin is the largest coal-producing site in India. The basin has continual deposition of shale and a coal sequence with fine- to medium-grain sized sandstone-shale. Sandstone channel shaped-bedded means that it is sheet-shaped and channel-shaped. Shale beds are layered and sheetlike structures. Fractures are seen in thin to moderately thick coal facies. Details about the tectonics and stratigraphy of the region can be found in refs 69−71. Raniganj shales were collected from the Asansol area, eastern part of India, from both opencast and underground coal mines. The Raniganj Basin is a portion of the Damodar Valley basin located at a latitude of 23°22′−23°52′ N and a longitude of 86°36′−87°30′ E with an area of 1900 km^2. Sandstones with alteration in siltstones, thick coal seams, and carbonaceous shale are characterized in the Barakar Formation. The detailed petrography, stratigraphy, and tectonic studies for the organic matter from the Raniganj Basin are mentioned in refs 32, 72.

2.2. Sample Collection and Processing. The depth range of the samples that were acquired from SM vary between 180 and 538 m; the samples are represented as SM 1, SM 2, and SM 3. In contrast, the depth ranges of the samples from BK are between 225 and 443 m; the samples are represented as BK 1, BK 2, BK 3, BK 4, BK 5, and BK 6, as mentioned below in Table 1. Shale cores were collected and preserved in an airtight bag to avoid any contamination. The samples were pulverized using an agate mortar, and a <75 μm grain size fraction was retained using a copper sieve (ASTM no. 200), which was used for the experimental analysis of X-ray diffraction (XRD), Rock-Eval pyrolysis, and LPGA method.

2.3. Determining Mineralogy and Organic Matter Composition. To evaluate the diffractograms in a PANalytical X'Pert Pro instrument, 2−5 mg of powdered samples was placed uniformly on the sample holder. The peaks for mineral matters were identified within the scanning range (2θ) of 5 to 70° with a scan step of 0.0130°/s. This instrument was analyzed using a Cu anode and a 40 kV maximum operating voltage. The diffractogram peak for mineral matter was analyzed using the HighScore Plus software suite.

Source-rock geochemical characterization of shales was performed using a Rock-Eval 6 device. Revised protocols, as developed by Hazra et al.[33,74,75] for accurate estimation of TOC, were followed to analyze the shales. To determine the characteristics of the potential source rocks, 5−10 mg of samples was used for analysis. The powdered samples were

https://doi.org/10.1021/acs.energyfuels.3c03374
Energy Fuels 2024, 38, 3833−3847

taken into crucibles and inserted initially into the pyrolysis chamber to be heated isothermally at 300 °C. The released free hydrocarbons (HCs) were carried by the N_2 gas and detected by a flame ionization detector (FID); they are represented as the "S_1" peak. Following this, the shales were heated from 300 to 650 °C at a heating rate of 25 °C/min, at which organic matter breaks into HCs; these were again carried by N_2 gas and detected by the FID, and they are presented as the "S_2" peak. T_{max} (the temperature at which the HC's generation at the S_2 stage is maximum) was recorded and allowed to investigate the organic matter thermal maturity levels within the studied shales. Similarly, oxygenated compounds in organic matter decomposed in the pyrolysis stage to generate CO_2 and CO were detected by the infrared cell and represented as "S_3". The carbon, which is generated under S_1, S_2, and S_3 curves, together yields the pyrolyzable carbon (PC) fraction. After the pyrolysis process, samples were shifted to the oxidation chamber, where they were heated under an oxidizing environment, which generates information about the amount of residual carbon (RC) in shales. TOC is the summation of PC and RC.

Other important indices calculated are as follows:

$$\text{hydrogen index(HI)} = [(S_2/\text{TOC}) \times 100] \quad (1)$$

$$\text{oxygen index(OI)} = [(S_3/\text{TOC}) \times 100] \quad (2)$$

2.4. Low-Pressure Gas Adsorption (LPGA). LPGA is the most effective method applied to illustrate the proxies of micropore and mesopore attributes such as SSA, PSD, and PV in shales. It is performed using a Quantachrome Autosorb IQ single-station physisorption device. The collected samples were pulverized to <75 μm. In a glass cell, 2−3 g of powdered samples was loaded and degassed at a pressure of 10^{-4} Torr and 110 °C for 12 h to eliminate the moisture content that was present in shale pores.[43,44,76,77] According to Singh et al.,[78] it is important to select the appropriate degassing temperature to minimize the error in the determination of pore attributes. Several researchers have reported the similar degassing temperature procedure of 110 °C, which is suitable to remove the moisture content and lower hydrocarbons without any alteration of pores in shales.[76,77] Singh et al.[78] and Chandra et al.[14] have shown the alteration in pore attributes due to breakdown of organic matter in shales with an increase in the degassing temperature from 110 to 200 and 300 °C and concluded that 110 °C is the most ideal degassing temperature without altering the solid organic matter in shales. Some researchers have also applied the degassing temperature of 250 °C[61] where the mass change in solid organic matter is minimal (∼1−2%); however, this observation was found to fail with shales of lower thermal maturity. Therefore, to keep uniformity in the degassing procedure, 110 °C is widely accepted, which causes a minimal mass change in solid organic matter. Several researchers[61,78] showed that the degassing temperature exerts a strong effect on the shale pore dimensions. The mesopore identity changes to a macropore identity when there is a rise in the degassing temperature, from 110 to 200 °C, which results in a manifold increase in the pore width/diameter.[80] After every 15 min cycle, a leak test was conducted to ensure precise degassing without any alteration of the sample. After degassing, the samples were loaded into the analysis chamber with a relative pressure of $0.01 < P/P_o < 0.99$ at a liquid N_2 temperature of 77 K (−196 °C) for N_2 adsorption. N_2 gas with a purity of 99.995% was used as an adsorbate for the samples. For CO_2 gas adsorption, the relative pressure varied as $0.005 < P/P_o < 0.03$, and the saturation pressure of 26,610 Torr was considered for the experiments. In addition, a recirculating bath with a chemical composition that consisted of ethylene glycol and water (50:50) was used to maintain the temperature at 273 K (0 °C). When there is an increase in P/P_o, the adsorbate molecule occupies the higher energy sites on the adsorbent and forms consecutive layers, which exist in a dynamic equilibrium with the adsorbent phase. The presence of specific functional groups and free ions in shales interacts with N_2 molecules due to their quadrupolar nature and adsorbed to the accessible active sites in the sample. The N_2 molecule appears in a closely packed "liquid state" in a monolayer that is compatible with hydrocarbon surfaces. Molecules of N_2 are limited in their ability to probe the pores that are at less than 1.3 nm.[11,12,28] BET is a modified equation of Langmuir's kinetics adsorption theory, which is used to determine the SSA for fine powders and nonporous and porous materials. It is seen that the pore size distribution of narrow mesopores cannot be evaluated based on the Kelvin equation. Density functional theory (DFT) is independent of capillary condensation and can extensively be applied for spectra of micro- and mesopore range. Non-local DFT (NLDFT) and quenched-solid DFT (QSDFT)[79−81] are two of the most used submodels of DFT. NLDFT is established based on the concepts of classical and statistical thermodynamics. The model assumes that the solid adsorbate is in thermodynamic equilibrium with the gas adsorptive phases. The NLDFT model can be used to evaluate the PSD of complex pore networks from both the adsorption and desorption curves.[82] QSDFT is a modified version of NLDFT, which was introduced to account for the degree of roughness in the pore surface. In this study, N_2 and CO_2 gases were used as an adsorbate, while carbon (C) was used as an adsorbent. The thermodynamic interaction in DFT is more sensitive than the BJH model, which does not have any thermodynamic consideration of adsorbent−adsorbate interaction. Since the van der Waals force is more dominant in smaller pores and constricted channels, ignoring thermodynamics can cause significant error in estimating pore volumes. This is why QSDFT has better accuracy quantifying smaller pores. Organic carbon and clay minerals are the major contributors in shale; therefore, both C-based DFT and Si-based DFT were applied to the DFT model.[63] The model was restricted to obtain the PSD up to a range of 40 nm with the carbon-based DFT model compared to the Kelvin equation-based BJH model, which can go up to 200 nm. Since shale pores are majorly smaller mesopores or micropores, DFT-based models, which focus on smaller mesopores, are well-suited. The wide spectrum of kernels with a specific adsorbent−adsorbent model can be adapted with different pore shapes for more accurate PSD calculations. The micropore SSA and the micropore volume in CO_2 adsorption were calculated using Dubinin−Radushkevich (D−R) and Dubinin−Astakhov (D−A) equations.

3. RESULTS

3.1. Mineral Composition. The results that were obtained from the XRD analysis of shales are represented below (Table 1). The samples have a substantial amount of quartz and clay mineral contents. Samples SM 3 and BK 2 show the maximum content of clay minerals, whereas samples SM 1 and BK 6 have a minimum content of clay minerals. Although muscovite is absent in SM 3 and BK 2 shales, feldspar is absent in SM 1 and SM 3. In contrast, BK and SM shales show a significant concentration of muscovite (except BK 2 and SM 3), while

https://doi.org/10.1021/acs.energyfuels.3c03374
Energy Fuels 2024, 38, 3833−3847

Table 2. Source-Rock Geochemical Properties for the Studied Shales

sample name	S_1 (mg HC/g rock)	S_2 (mg HC/g rock)	T_{max} (°C)	PC (wt %)	RC (wt %)	TOC (wt %)	HI (mg HC/g TOC)	OI (mg CO_2/g TOC)
SM 1	0.15	4.38	428	0.5	6.92	7.42	59	25
SM 2	0.30	10.73	428	1.06	10.73	11.79	91	16
SM 3	0.05	0.44	441	0.05	0.99	1.04	42	15
BK 1	0.23	4.86	441	0.52	5.51	6.03	81	19
BK 2	0.77	9.24	445	0.93	9.78	10.71	86	8
BK 3	0.45	5.87	445	0.67	6.11	6.78	87	16
BK 4	0.44	9.11	438	0.89	6.43	7.32	124	14
BK 5	0.36	7.94	444	0.75	5.78	6.53	122	10
BK 6	0.46	6.46	447	0.63	6.34	6.97	93	12

feldspar is absent in SM 2 and all BK shales. The shales are also composed of siderite (except SM 1 and SM 3).

3.2. Thermal Maturity and Organic Richness. The results that were obtained from the Rock-Eval analysis are presented in Table 2. T_{max} reveals the contrasting thermal maturities of the studied shales. While shales from the Korba Basin (SM 1−SM 3) are "immature" to "early mature", the samples from the Raniganj Basin (BK 1−BK 6) are "early mature" to "peak mature", i.e., marked by a higher thermal maturity level. The HI and OI of the samples from both the basins vary between 42 and 124 mg HC/g of TOC and 8 and 25 mg CO_2/g of TOC, respectively, which indicates an input of the dominantly kerogen type III (as represented below in Figure 2).

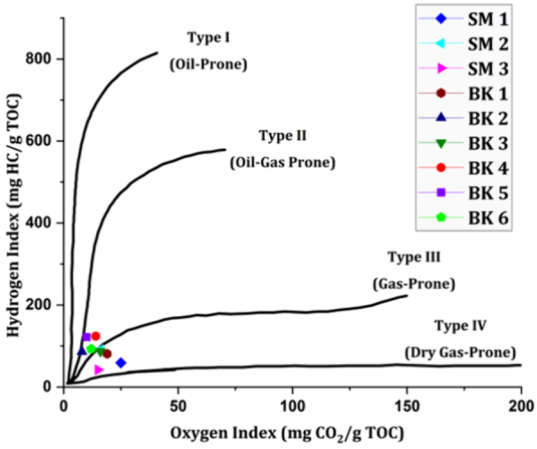

Figure 2. Modified van Krevelen diagram for the studied shales.

3.3. Pore Characteristics. N_2 adsorption for the shales shows an isotherm of type IV with H3 hysteresis for the Raniganj Basin and Korba Basin (Figure 3a,c). The sample shows the tensile strength effect (TSE) within P/P_o of ∼0.45−0.55 due to cavitation in pores.[83] Among Raniganj shales, BK 5 has the maximum adsorption capacity at 31.55 cc/g, while BK 2 and BK 3 have the least at 22.11 and 22.27 cc/g, respectively. In Korba shales, SM 1 shows a maximum adsorption capacity of 30.47 cc/g, which is slightly less than the maximum value of Raniganj shales. In contrast, SM 3 has the least adsorption capacity of 25.61 cc/g.

The CO_2 adsorption isotherms from Raniganj and Korba Basins show type II isotherms (Figure 3b,d), which indicates the filling of active micropore sites. In micropore filling, initially, a monolayer forms that occupies the active site on shales. The shales from the Korba Basin (3.93 cc/g) show greater adsorption potential than those from the Raniganj Basin (3.22 cc/g) from P/P_o = 0.0003−0.03, which reveals the higher filling of micropores in the case of the Korba Basin. The Raniganj shales show a uniform growth in the gas volume adsorbed with an increase in the pressure; this growth denotes uniform filling in shale pores.

3.3.1. Micro- and Mesopore Attributes. Pore attributes such as TPV and SSA for nanopores were estimated by using combined CO_2 and N_2 gas adsorption. The mesopore SSA was evaluated using the BET equation, which is a modified equation of the Langmuir kinetics theory of gases for the monolayer filling of pores. In this case, it was assumed that the gas molecules adsorbed to the solid surfaces that occupied the active monolayer sites, and the enthalpy of adsorption decreased when the layer increased. The maximum BET SSA is shown by BK 5, whereas BK 3 has the minimum BET SSA among all the samples. The BET SSA varies between 15.14 and 31.65 m^2/g, in which shales from the Raniganj Basin have a higher average BET SSA than shales from the Korba Basin as mentioned in Table 4. To evaluate the PSD for CO_2 and N_2 adsorption from adsorption curves, CO_2-DFT and QSDFT models, respectively, are applied. The maximum total pore volume (TPV) is shown by SM 3, while BK 6 has the minimum TPV among the samples. TPV for shales varies between 0.05 and 0.092 cc/g as mentioned below in Table 4. Shales from the Korba Basin have a significantly higher micropore volume than shales from the Raniganj Basin. The maximum average pore width (PW) is shown by SM 1, whereas BK 5 indicates the minimum average PW. The average PW for the samples varies between 6.17 and 10.40 nm.

3.3.2. Pore Size Distribution (PSD). Mesopore distribution is evaluated using N_2 adsorption isotherms, explaining the pore structural characteristics of shales. PSD is computed as the derivative function of the pore volume to the logarithm of the pore width ($dV/d\log D$), which illustrates spectra of pore distribution in the shales. The DFT model accounts for an interaction between the adsorbate and the adsorbent, which provides better accuracy in determining smaller mesopores. The PSD in shales is determined using the QSDFT model, which assumes that a solid is a component that has homogeneous density. The surface roughness of the distributed solid atoms is due to heterogeneity. The addition of the surface roughness correction factor to PSD calculation improves the knowledge of pore characteristics in the NLDFT theory. Studies show that QSDFT has a better fit of the measured adsorption isotherm, which reduces errors in determining the PSD. The PSD calculation using a desorption branch provides certain artifacts due to the forced closure of the pore spaces. A combination of PSD for both the CO_2 and N_2 experimental adsorption isotherm is shown below, in Figure 4. In CO_2 PSD, SM 2 shows multimodal PSD, with the maximum peaks at around 0.3−0.6 nm among the shale samples. A similar PSD behavior is seen in

https://doi.org/10.1021/acs.energyfuels.3c03374
Energy Fuels 2024, 38, 3833−3847

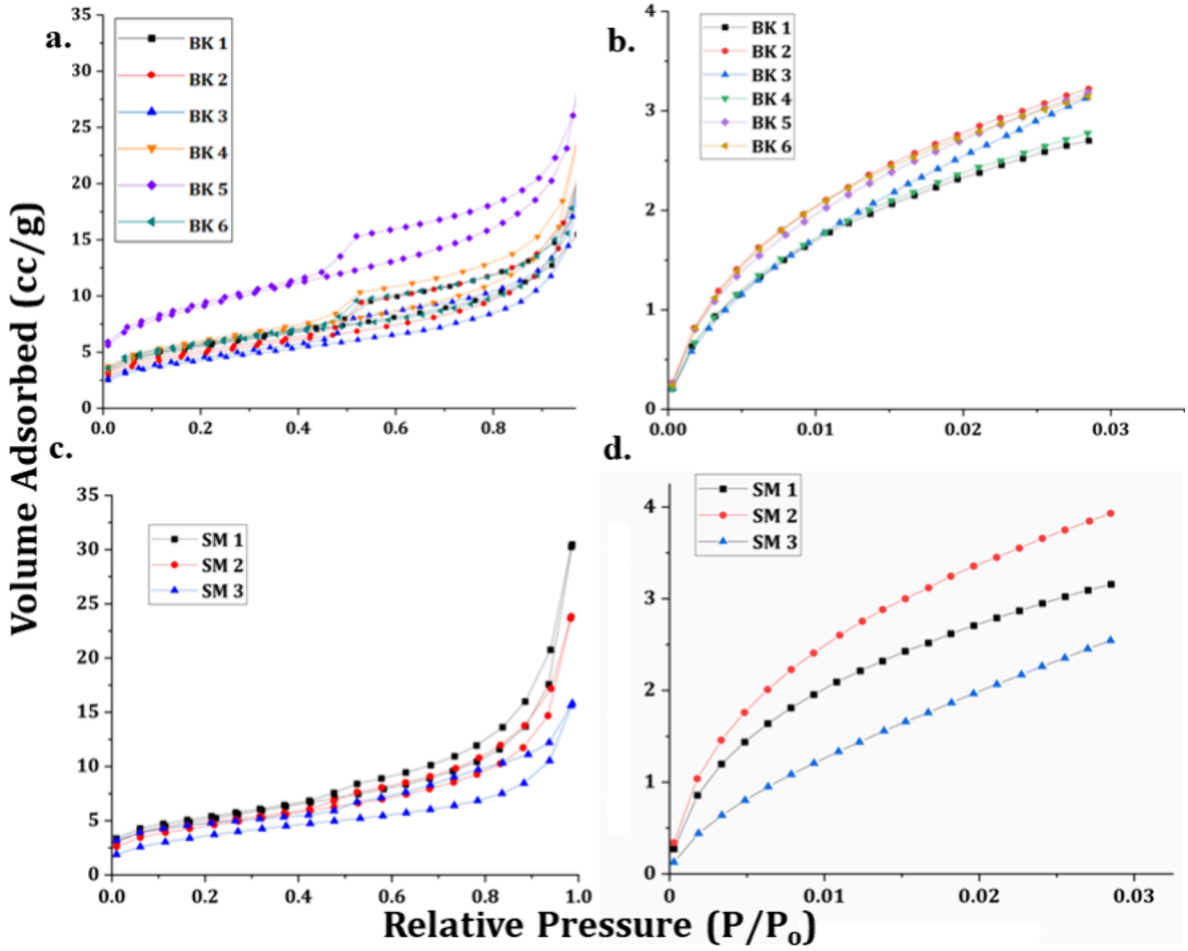

Figure 3. Isotherms for N_2 gas adsorption and desorption trends for (a) (top left) Barakar Basin and (c) (bottom left) Korba Basin; isotherms for CO_2 gas adsorption trends for (b) (top right) Barakar Basin and (d) (bottom right) Korba Basin.

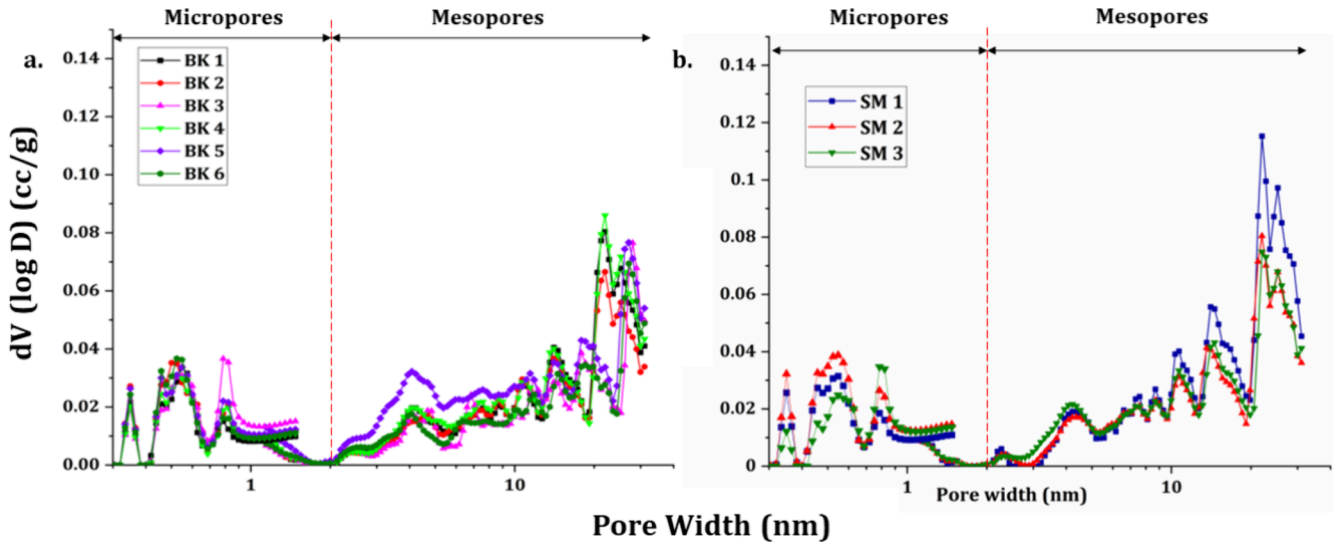

Figure 4. Combined QSDFT PSD plot (from the adsorption branch) for (a) (left) Barakar Basin and (b) (right) Korba Basin.

SM 1, SM 2, and SM 3, with peaks at around 0.3−0.6 nm. The samples of BK shale also show a peak range of around 0.3−0.7 nm. They also show pore size peaks at around 0.3−0.7 nm, where SM 2 and BK 2 peaks are the most dominant among the respective basins.

In the N_2 PSD, BK 1, BK 2, and BK 4 show a sharp peak at around 20−25 nm, while the other samples from BK shales shift slightly to the right and have a significant PSD at around 25−30 nm; this may be due the higher siderite content in samples (BK 1, BK 2, and BK 4). The highest peak at around 20−25 nm is shown by SM 1, which is similar to all other SM shales. The peak

https://doi.org/10.1021/acs.energyfuels.3c03374
Energy Fuels 2024, 38, 3833−3847

curve for the SM shales show higher values than that of BK shales.

3.3.3. Fractal Dimension (D_s). The fractal dimension (D_s) is one of the metrics that are used to characterize complexity in pore surfaces of sedimentary rocks at different length scales. It describes the pore formation and the degree of self-similarity in a structure across different scales. The surface fractal is calculated using the N_2 adsorption isotherm in nanoporous rocks, such as shale. The fractal dimension depicts the effect of the organic matter maturity in shales. Fluid flow kinetics and gas exploration in a shale reservoir are significantly impacted by the surface irregularity in shales and are independent of their depositional nature. The fractal dimension model such as the FHH model operates based on the equation mentioned in Table 3 in the

Table 3. Fractal Dimensions for the Korba and Raniganj Basins[a]

	$D_1 = (3 + S_2)$		$D_2 = (3 + 3S_1)$	
sample name	$0.01 < (\frac{P}{P_o}) < 0.5$	R^2	$0.5 < (\frac{P}{P_o}) < 0.98$	R^2
SM 1	2.55	0.99	1.89	0.99
SM 2	2.53	0.99	1.96	0.99
SM 3	2.57	0.98	2.1	0.99
BK 1	2.57	0.98	2.06	0.99
BK 2	2.55	0.98	2.05	0.99
BK 3	2.54	0.99	1.98	0.98
BK 4	2.56	0.99	2.06	0.99
BK 5	2.59	0.98	2.26	0.99
BK 6	2.62	0.97	2.12	0.98

[a]Calculated using the FHH methods.

condensation regime. It must be noted that these mathematical equations are based on Kelvin's equation, considering that their mathematical and physical configurations are similar.

The plot fitting to the curve shows linear trends, while certain shale-fluid interactions show a little deviation from the linear trend, as mentioned in the Supporting Information. This uncertainty in linear fitting is mostly due to pore-space heterogeneity or anisotropy in shale. The difference in the pore-filling process defines two distinct fractal dimensions in the shale samples. D_s is directly proportionate to the active surface sites present in the adsorbate. At the $0.01 < P/P_o < 0.5$ regime, the van der Waals force accounts for the adsorbate and adsorbent due to low surface tension, while at the $0.5 < P/P_o < 0.99$ regime, surface tension dominates, and the capillary condensation phenomenon has a significant role in the determination of fractal characteristics. D_s in the capillary condensation regime is given as an equation below.

$$\ln\left(\frac{V}{V_m}\right) = C + A\ln\left[\ln\left(\frac{P}{P_o}\right)\right] \quad (3)$$

At a low P/P_o regime,

$$A = (D_s - 3) \quad (4)$$

At a high P/P_o regime,

$$A = (D_s - 3)/3 \quad (5)$$

Table 3 shows that the values of D_{FHH} at lower and higher pressures are different, which signifies the nonlinearity in the adsorption isotherm graphical plot between $\ln(\frac{V}{V_m})$ vs $\ln(-\ln(\frac{P}{P_o}))$ in Figures S1 and S2 mentioned in the Supporting Information. The D_{FHH} value shows 2.53−2.62 at the low-pressure regime ($0.01 < P/P_o < 0.5$) and 1.89−2.26 at the higher-pressure regime ($0.5 < P/P_o < 0.98$). Samples BK 6 and SM 3 have the maximum D_{FHH} and SM 1 and BK 3 shows the minimum D_{FHH} at lower- and higher-pressure regimes, respectively, in the respective basins. In Table 3, SM 1, SM 2, and BK 3 show D_s values lesser than 2, which is lower than the theoretical lower limit of the surface fractal dimension. The reason for a lower D_s value (<2) in Table 3 can be explained from the concept of the FHH fractal dimension. Since the adsorption mechanism in smaller and coarser mesopores is dominated by the van der Waals force and capillary condensation, respectively, the FHH fractal fit has different slopes for smaller and larger pores. Hence, the fractal dimension (D_s) calculated using the N_2 adsorption isotherm has been divided into two relative pressure regimes, namely, D_1 ($0.01 < P/P_o < 0.5$) and D_2 ($0.5 < P/P_o < 0.99$). At the lower-pressure regime, the interaction of the solid surface and gas interface is dominated by the van der Waals force of attraction, which makes the fluid interface replicate the surface roughness. Therefore, the D_s in this case is calculated using eq 4. Meanwhile, at the higher-pressure regime, the interaction between the solid and gas phase is dominated by the surface tension (or capillary condensation), where the gas interface moves away from the solid surface and thus reduces the interface area. Therefore, the D_s in this case is calculated using eq 5. However, in the intermediate-pressure regime that occurs between eqs 4 and 5, the multilayer formation (or second layer) starts early, which makes the van der Waals of attraction weak and eq 4 ineffective. Therefore, the D_s value in the intermediate-pressure regime is calculated using only eq 5 and neglecting eq 4. Therefore, this phenomenon underestimates the fractal dimension and provides the D_s value of less than 2. A similar result has been obtained in other studies as well.[84−87] The result of the fractal dimension model varies for all of the samples, and it is important to contrast the performance to comprehend the pore structure of collected shales.

4. DISCUSSION

The combined CO_2−N_2 LPGA method is applied to characterize the pore attributes of shales collected from different depths of the Permian age. This method confers an understanding of the important roles of clay minerals and organic matter in the contribution of the total porosity in shales with the changes in depth. The content of mineral matter, which is calculated using XRD analysis, provides the quantification of silicates, carbonates, and clay minerals in shale. The Rock-Eval method provides information about thermal maturity and the organic matter types in shale samples. The micropore SSA and microporous PV, which are calculated using the D−R and D−A methods respectively, show that SM 2 and SM 3 have the highest contribution toward the micropore SSA and microporous PV, respectively. PSD from the N_2 adsorption isotherm that is determined by using the QSDFT method shows a multimodal peak representation in the samples. The highest peak between 20 and 25 nm is shown by SM shales, while the highest peak of BK shales is between 20−25 and 25−30 nm for some samples influenced by the presence of the siderite content. In CO_2-DFT, the samples show similar multimodal characteristics: the highest peak between 0.3 and 0.6 nm is seen for SM 1, SM 2, and SM 3, while BK shales show a peak at around 0.4 to

https://doi.org/10.1021/acs.energyfuels.3c03374
Energy Fuels 2024, 38, 3833−3847

Table 4. Pore Attributes of Shale Samples Collected from the Korba and Raniganj Basins

	specific surface area (SSA) (m^2/g)		average pore width (PW) (nm)	total pore volume (TPV) (cc/g)		
sample	micropore	mesopore	mesopore	micropore	mesopore	micro + mesopores
SM 1	30.67	18.12	10.40	0.015	0.047	0.062
SM 2	38.02	16.11	9.15	0.020	0.037	0.057
SM 3	25.72	20.26	7.82	0.053	0.039	0.092
BK 1	27.06	19.59	7.99	0.014	0.040	0.054
BK 2	31.68	17.31	7.90	0.017	0.034	0.051
BK 3	33.13	15.14	9.10	0.034	0.034	0.068
BK 4	28.02	19.95	8.11	0.015	0.040	0.055
BK 5	30.80	31.65	6.17	0.018	0.049	0.067
BK 6	31.84	19.37	7.31	0.015	0.035	0.050

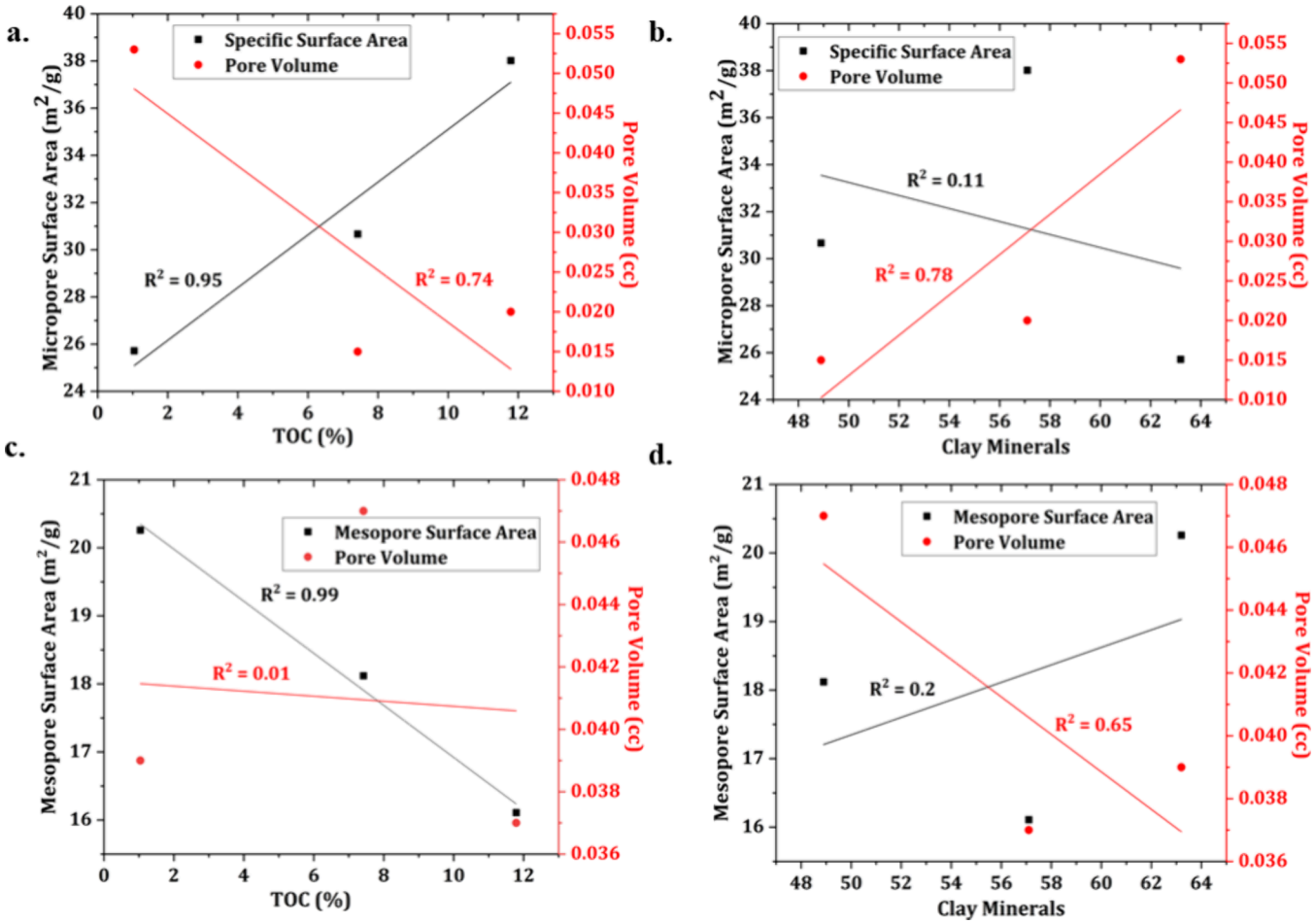

Figure 5. Correlation of (a) micropore SA with TOC, (b) micropore SA with the clay mineral content, (c) mesopore SA with TOC, and (d) mesopore SA with the clay minerals content for SM shales.

0.7 nm. Sample BK 4 shows the highest peaks as a consequence of its high organic matter and clay mineral content.

Table 4 shows the pore characteristics of shales from the Korba and Raniganj Basins. In SM shales, SM 1 and SM 2 have a higher microporous SSA than SM 3, which could be due to the high TOC value. This indicates a better relationship between the organic matter composition and the microporosity attributes. In BK shales, despite the high TOC values of BK 2 and BK 4, less SSA than that of BK 3 is seen, which indicates the influence of the siderite presence on the microporosity of the samples. BK samples comprise a more significant amount of siderite than SM samples, which indicates less microporosity in the samples. Moreover, BK and SM shales show a confident correlation with the clay mineral content. In samples BK 2 and BK 4, despite their high content of clay minerals, a low mesopore SSA is seen; this could also be attributed to the significant amount of siderite in the BK shales. On the contrary, BK 5 shows the maximum BET SSA due to the low siderite content compared with all BK shales. The result also implies that in the BK and SM samples, there is an inverse correlation between the mesopore SSA and the average PW.

Figures 5 and 6 display a correlation between TOC and clay mineral composition along with shale pore attributes (micro- and mesopores) for both Korba and Raniganj Basins. Figure 5a,c depicts that the micro- and mesopore SA values have an excellent fitting with 95 and 99%, respectively, while the micro-

https://doi.org/10.1021/acs.energyfuels.3c03374
Energy Fuels 2024, 38, 3833−3847

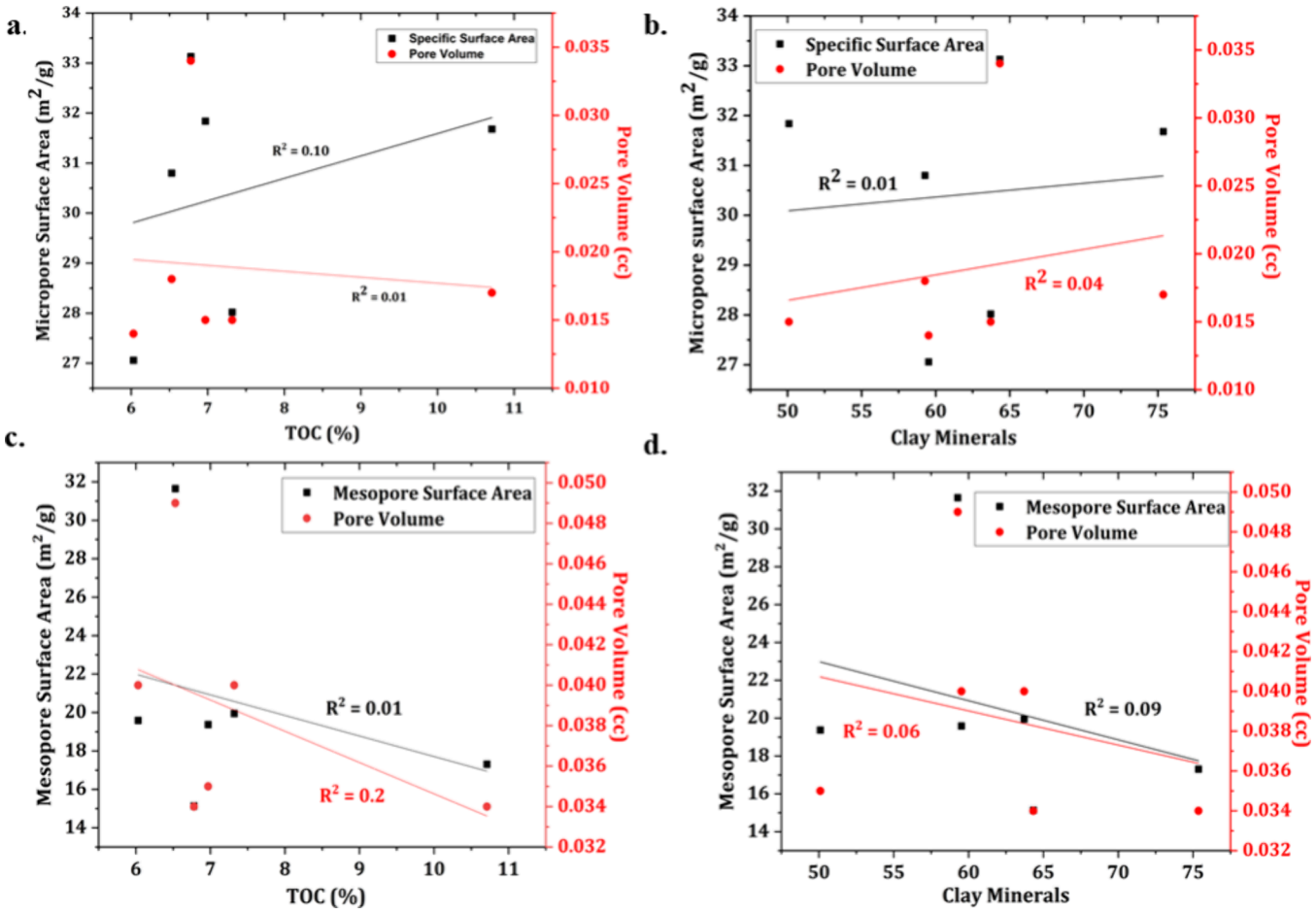

Figure 6. Correlation of (a) micropore SA with TOC, (b) micropore SA with the clay mineral content, (c) mesopore SA with TOC, and (d) mesopore SA with the clay mineral content for BK shales.

and mesopore volume shows a good fitting (74%) and weak fitting (1%), respectively, with TOC for SM shales. The nanopore abundance in organic matter provides it with primary sites for gas storage and production. Figure 5b,d illustrates a weak fitting of micro- (11%) and mesopore SA (20%) with clay minerals for both SM and BK shales respectively. Additionally, there is a good relationship between the micropore (78%) and mesopore volume (65%) with clay minerals. The results explain that clay minerals have a significant contribution to gas storage due to their clay structure. Figure 6 shows that micro- and mesopore attributes have a weak correlation for both TOC and clay mineral composition. However, the mesopore volume for BK shales (20%) is higher than for SM (1%) shales, which signifies that BK shales have a higher affinity toward mesopores. TOC values for SM shales are higher than for BK shales, which significantly results in higher micropore attributes. Furthermore, TOC values for BK shales are relatively varying between 6 and 7 (except BK 2), which implies narrow SA and PV (except BK 5) in BK shales compared with SM shales. The least siderite content results in a higher SA and PV in sample BK 5.

Figures 7 and 8 explain the determination of the fractal dimensions (D_s) with pore attributes, TOC, and clay minerals for SM and BK shales, respectively. To determine the D_s, it has been divided into two relative pressures (P/P_o) regimes: the low-pressure regime ($0.01 < P/P_o < 0.5$) and the high-pressure regime as explained earlier. Figure 7a shows an excellent (99%) and weak correlation (32%) between D_s and micropore SA at low- and high-pressure regimes, respectively. However, D_s becomes more significant with the mesopore SA as shown in Figure 7b, specifically at high-pressure regimes. Additionally, D_s happens to be more dominant with pore width over the high-pressure regimes in Figure 7c. Here, we can observe a reverse trend between the mesopore SA and the average pore width. Figure 7d,e illustrates a correlation between D_s and organic matter and clay minerals for SM shales. Furthermore, it depicts that the TOC has a higher influence on D_s compared with clay composition, especially at lower-pressure regimes. Figure 8a shows an insignificant correlation between D_s and micropore SA at both low- and high-pressure regimes. However, D_s is more substantial with mesopore SA in Figure 8b, especially at a high-pressure regime (92%). Additionally, an opposite trend is observed between the pore width and the mesopore SA, similar to SM shales in Figure 8c. Figure 8d,e establishes a correlation between D_s and organic matter and clay minerals for BK shales, which reveals that the clay minerals have a higher consequence on D_s as compared with TOC, significantly at a lower-pressure regime.

Several researchers have provided the similar correlation and fitted the curve with the coefficient of determination (R^2).[63,88−90] Wang et al.[84] showed a correlation between the fractal dimension and the TOC content, mineral matters, and pore structure parameters. It reveals a good correlation for the BET surface area and a negative correlation with the average pore diameter, while no correlation has been shown between the

https://doi.org/10.1021/acs.energyfuels.3c03374
Energy Fuels 2024, 38, 3833−3847

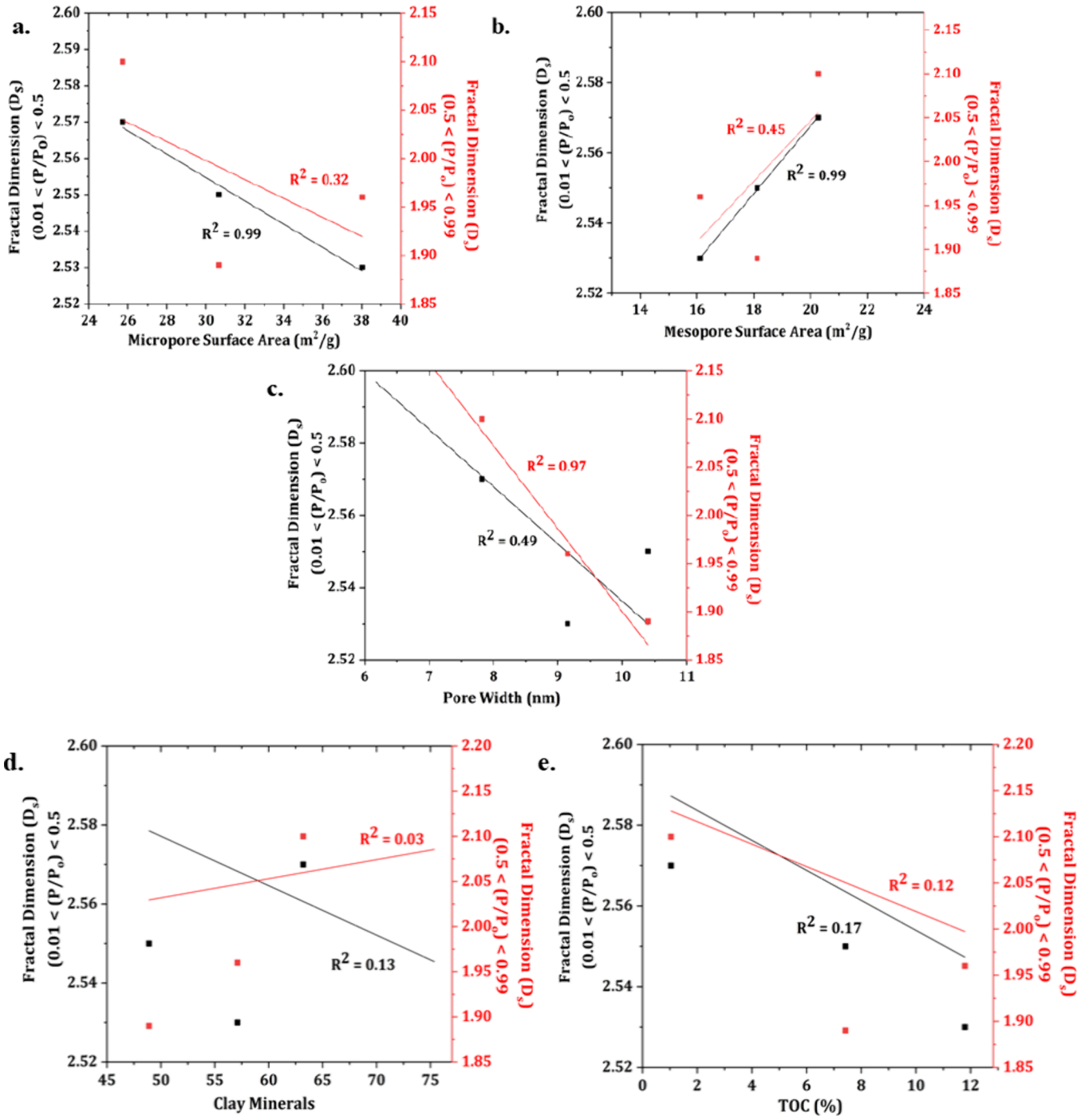

Figure 7. Correlations between fractal dimension and (a) micropore SA, (b) mesopore SA, (c) average pore width, (d) clay minerals, and (e) TOC for SM shales. Representative colors for the fractal dimension at different (P/P_o) regimes mentioned in the plots correspond to the respective *Y*-axes.

TOC content, mineral matter, and fractal dimension. Liu et al.[85] have shown the correlation between the pore structure parameter with the TOC content and mineral composition while also the relationship between the fractal dimension and the mineralogy content. The plot shows a good correlation (47.65−75.23%). Bhapkar et al.[54] determined the correlation between the influence of TOC and pore attributes. It also reveals a good correlation range from 27 to 80%. Li et al.[91] revealed a relationship between pore structure characteristics and mineral contents. It shows a positive correlation between the pore attributes and the TOC content, while it shows a negative correlation between the pore attributes and the clay content. Since the correlations derived from our study follow similar global trends, we believe the correlations to be valid within the constraints of our experimental limitations.

5. CONCLUSIONS

This study provides an understanding of the comparative pore attributes and pore accessibility of shales from Barakar formations collected from two proliferous basins, namely, the Korba and Raniganj Basins in India. The research was conducted to investigate the gas exploration potentials in these basins. The following are the key points of this research.

https://doi.org/10.1021/acs.energyfuels.3c03374
Energy Fuels 2024, 38, 3833−3847

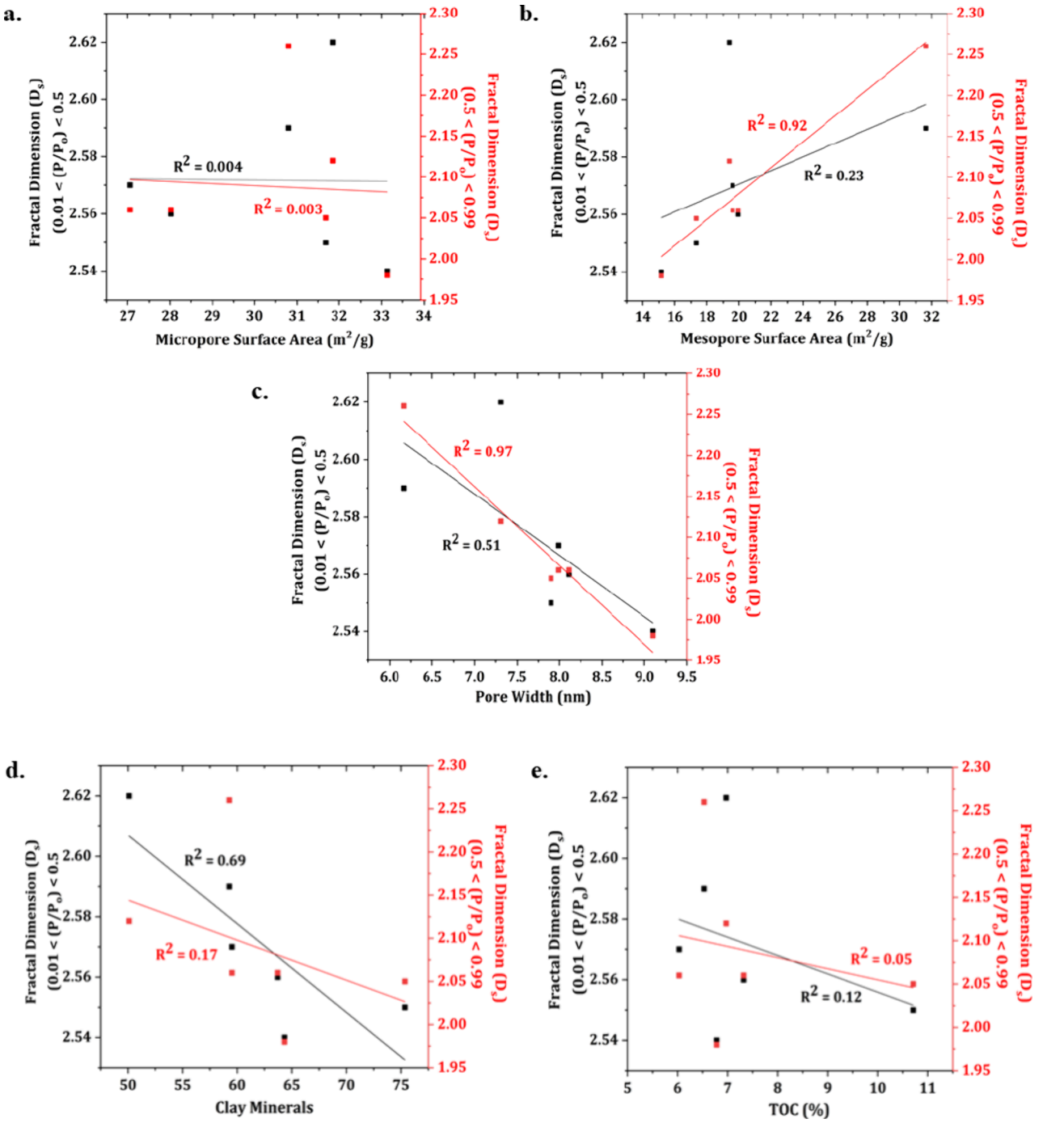

Figure 8. Correlations between the fractal dimension model and (a) micropore SA, (b) mesopore SA, (c) average pore width, (d) clay minerals, and (e) TOC for BK shales.

1. Mesopore pore size distribution (PSD) for both collected shales shows a similar trend. However, the presence of siderite shows a variance in the peaks for some shales (BK1, BK2, and BK4), which are slightly lagging, compared with the shales (BK3, BK5, and BK6) having a low siderite content. Micro- and mesopore PSD in shales can be interrelated with the TOC and clay minerals, respectively.
2. Among the studied samples collected from different locations across various depths, Korba shales are richer in micropore volume than Raniganj shales, thereby a higher total pore volume (micro- and mesopores). Korba shales signify a better choice for the shale gas recovery than Raniganj shales.
3. The fractal dimension (D_s) is determined using the FHH model, which reveals that D_s has an excellent correlation with micro- and mesopore attributes at low relative pressure regimes for Korba shales, while Raniganj shales show a strong affinity toward mesopores at high relative pressure regimes.
4. Korba Basin shales reveal higher micropore attributes than the Raniganj Basin shales, which makes it suitable for shale gas storage and production. Nevertheless, a comprehensive inference on these basins could be

https://doi.org/10.1021/acs.energyfuels.3c03374
Energy Fuels 2024, 38, 3833−3847

conclusive, only after considering other reservoir conditions and parameters. Therefore, these research findings will be crucial to unlocking the technical feasibility of gas storage capacity for other basins in India as well.

■ ASSOCIATED CONTENT

Supporting Information

The Supporting Information is available free of charge at https://pubs.acs.org/doi/10.1021/acs.energyfuels.3c03374.

Fractal dimension plots for the shale samples calculated using the FHH model (PDF)

■ AUTHOR INFORMATION

Corresponding Author

Vikram Vishal − *Computational and Experimental Geomechanics Laboratory, Department of Earth Sciences, National Centre of Excellence in Carbon Capture and Utilization, and Interdisciplinary Programme in Climate Studies, Indian Institute of Technology Bombay, Mumbai 400076, India;* orcid.org/0000-0002-0896-7844; Phone: +91-22-2576-7254; Email: v.vishal@iitb.ac.in

Authors

Shubham Kumar − *Computational and Experimental Geomechanics Laboratory, Department of Earth Sciences, Indian Institute of Technology Bombay, Mumbai 400076, India; Department of Civil Engineering, Faculty of Engineering, Monash University, Melbourne, Victoria 3800, Australia*

Debanjan Chandra − *Department of Geoscience and Engineering, Delft University of Technology, Delft 2628 CN, The Netherlands*

Bodhisatwa Hazra − *CSIR-Central Institute of Mining and Fuel Research, Dhanbad 826015, India; Institute of Geosciences, Marine and Land Geomechanics and Geotectonics, Christian-Albrechts-Universität, Kiel 24118, Germany;* orcid.org/0000-0002-3462-7552

Ranjith Pathegama Gamage − *Department of Civil Engineering, Faculty of Engineering, Monash University, Melbourne, Victoria 3800, Australia;* orcid.org/0000-0003-0094-7141

Complete contact information is available at: https://pubs.acs.org/10.1021/acs.energyfuels.3c03374

Notes

The authors declare no competing financial interest.

■ ACKNOWLEDGMENTS

The authors acknowledge IITB-Monash Research Academy, for the facilities used for the experiments. The authors would like to acknowledge support from DST, India supported by the National Center of Excellence in Carbon Capture and Utilization (DST/TMD/CCUS/CoE/202/IITB). The authors also acknowledge Geological Survey of India (GSI) for providing the copyright permission to use the District Resource Map of Korba, Chhattisgarh. S.K. would like to acknowledge the Prime Minister's Research Fellowship (PMRF) from the MHRD, Govt. of India for funding the doctoral program.

■ ABBREVIATIONS:

P = vapor pressure (in Torr)
P_o = condensation pressure of nitrogen at 77 K (in Torr)
V = volume of nitrogen adsorbed on the adsorbent at an equilibrium pressure (P/P_o) (in cc)
V_m = volume of gas at monolayer adsorption (in cc)
A = power-law exponent depending on D_s
PC = pyrolysis carbon
T_{max} = thermal maturity
PC = pyrolyzable carbon
RC = residual carbon
TOC = total organic carbon
HI = hydrogen index
OI = oxygen index

■ REFERENCES

(1) Vishal, V.; Ranjith, P. G.; Singh, T. N. CO2 Permeability of Indian Bituminous Coals: Implications for Carbon Sequestration. *Int. J. Coal Geol* **2013**, *105*, 36−47.

(2) Vishal, V.; Singh, L.; Pradhan, S. P.; Singh, T. N.; Ranjith, P. G. Numerical Modeling of Gondwana Coal Seams in India as Coalbed Methane Reservoirs Substituted for Carbon Dioxide Sequestration. *Energy* **2013**, *49* (1), 384−394.

(3) Bui, M.; Adjiman, C. S.; Bardow, A.; Anthony, E. J.; Boston, A.; Brown, S.; Fennell, P. S.; Fuss, S.; Galindo, A.; Hackett, L. A.; Hallett, J. P.; Herzog, H. J.; Jackson, G.; Kemper, J.; Krevor, S.; Maitland, G. C.; Matuszewski, M.; Metcalfe, I. S.; Petit, C.; Puxty, G.; Reimer, J.; Reiner, D. M.; Rubin, E. S.; Scott, S. A.; Shah, N.; Smit, B.; Trusler, J. P. M.; Webley, P.; Wilcox, J.; Mac Dowell, N. Carbon Capture and Storage (CCS): The Way Forward. *Energy Environ. Sci.* **2018**, *11* (5), 1062−1176.

(4) Zhang, X.; Jin, C.; Zhang, D.; Zhang, C.; Ranjith, P. G.; Yuan, Y. Carbon Dioxide Flow Behaviour in Macro-Scale Bituminous Coal: An Experimental Determination of the Influence of Effective Stress. *Energy* **2023**, *268*, No. 126754.

(5) Bernard, S.; Horsfield, B.; Schulz, H. M.; Wirth, R.; Schreiber, A.; Sherwood, N. Geochemical Evolution of Organic-Rich Shales with Increasing Maturity: A STXM and TEM Study of the Posidonia Shale (Lower Toarcian, Northern Germany). *Mar Pet Geol* **2012**, *31* (1), 70−89.

(6) Liu, K.; Ostadhassan, M.; Zhou, J.; Gentzis, T.; Rezaee, R. Nanoscale Pore Structure Characterization of the Bakken Shale in the USA. *Fuel* **2017**, *209*, 567−578.

(7) Middleton, R. S.; Gupta, R.; Hyman, J. D.; Viswanathan, H. S. The Shale Gas Revolution: Barriers, Sustainability, and Emerging Opportunities. *Appl. Energy* **2017**, *199*, 88−95.

(8) Vishal, V.; Verma, Y.; Chandra, D.; Ashok, D. A Systematic Capacity Assessment and Classification of Geologic CO2 Storage Systems in India. *International Journal of Greenhouse Gas Control* **2021**, *111*, No. 103458.

(9) IEA (2020), *Gas 2020*, IEA: Paris https://www.iea.org/reports/gas-2020, License: CC BY 4.0.

(10) Ross, D. J. K.; Marc Bustin, R. The Importance of Shale Composition and Pore Structure upon Gas Storage Potential of Shale Gas Reservoirs. *Mar Pet Geol* **2009**, *26* (6), 916−927.

(11) Clarkson, C. R.; Freeman, M.; He, L.; Agamalian, M.; Melnichenko, Y. B.; Mastalerz, M.; Bustin, R. M.; Radliński, A. P.; Blach, T. P. Characterization of Tight Gas Reservoir Pore Structure Using USANS/SANS and Gas Adsorption Analysis. *Fuel* **2012**, *95*, 371−385.

(12) Kuila, U.; Prasad, M. Specific Surface Area and Pore-Size Distribution in Clays and Shales. *Geophys Prospect* **2013**, *61* (2), 341−362.

(13) Wang, S.; Feng, Q.; Zha, M.; Javadpour, F.; Hu, Q. Supercritical Methane Diffusion in Shale Nanopores: Effects of Pressure, Mineral Types, and Moisture Content. *Energy Fuels* **2018**, *32* (1), 169−180.

(14) Chandra, D.; Bakshi, T.; Vishal, V. Thermal Effect on Pore Characteristics of Shale under Inert and Oxic Environments: Insights on Pore Evolution. *Microporous Mesoporous Mater.* **2021**, *316*, No. 110969.

(15) Chalmers, G. R. L.; Bustin, R. M. The Organic Matter Distribution and Methane Capacity of the Lower Cretaceous Strata of Northeastern British Columbia, Canada. *Int. J. Coal Geol.* **2007**, *70* (1−3), 223−239.
(16) Rouquerol, F.; Rouquerol, J.; Sing, K. S. W.; Llewellyn, P.; Maurin, G. *Adsorption by Powders and Porous Solids Principles, Methodology and Applications* Second Edition; 2014 Academic Press. DOI: 10.1016/C2010-0-66232-8.
(17) Jarvie, D. M.; Hill, R. J.; Ruble, T. E.; Pollastro, R. M. Unconventional Shale-Gas Systems: The Mississippian Barnett Shale of North-Central Texas as One Model for Thermogenic Shale-Gas Assessment. *American Association of Petroleum Geologists Bulletin* **2007**, *91* (4), 475−499.
(18) Jarvie, D. M. Shale Resource Systems for Oil and Gas: Part 2—Shale-Oil Resource Systems. *AAPG Memoir* **2012**, *97*, 89−119.
(19) Mastalerz, M.; Schimmelmann, A.; Drobniak, A.; Chen, Y. Porosity of Devonian and Mississippian New Albany Shale across a Maturation Gradient: Insights from Organic Petrology', Gas Adsorption, and Mercury Intrusion. *Am. Assoc Pet Geol Bull.* **2013**, *97* (10), 1621−1643.
(20) Lahann, R.; Mastalerz, M.; Rupp, J. A.; Drobniak, A. Influence of CO2 on New Albany Shale Composition and Pore Structure. *Int. J. Coal Geol* **2013**, *108*, 2−9.
(21) Varma, A. K.; Biswal, S.; Hazra, B.; Mendhe, V. A.; Misra, S.; Samad, S. K.; Singh, B. D.; Dayal, A. M.; Mani, D. Petrographic Characteristics and Methane Sorption Dynamics of Coal and Shaly-Coal Samples from Ib Valley Basin, Odisha. *India. Int. J. Coal Geol* **2015**, *141−142*, 51−62.
(22) Vishal, V.; Chandra, D.; Bahadur, J.; Sen, D.; Hazra, B.; Mahanta, B.; Mani, D. Interpreting Pore Dimensions in Gas Shales Using a Combination of SEM Imaging, Small-Angle Neutron Scattering, and Low-Pressure Gas Adsorption. *Energy Fuels* **2019**, *33* (6), 4835−4848.
(23) Wilson, M. J.; Wilson, L. Clay Mineralogy and Shale Instability: An Alternative Conceptual Analysis. *Clay Miner* **2014**, *49* (2), 127−145.
(24) Chen, S.; Han, Y.; Fu, C.; Zhang, han; Zhu, Y.; Zuo, Z. Micro and Nano-Size Pores of Clay Minerals in Shale Reservoirs: Implication for the Accumulation of Shale Gas. *Sediment. Geol.* **2016**, *342*, 180−190.
(25) Zhang, T.; Ellis, G. S.; Ruppel, S. C.; Milliken, K.; Yang, R. Effect of Organic-Matter Type and Thermal Maturity on Methane Adsorption in Shale-Gas Systems. *Org. Geochem.* **2012**, *47*, 120−131.
(26) Curtis, M. E.; Ambrose, R. J.; Sondergeld, C. H.; Rai, C. S. Investigation of the Relationship between Organic Porosity and Thermal Maturity in the Marcellus Shale. *Society of Petroleum Engineers - SPE Americas Unconventional Gas Conference and Exhibition*, UGC 2011 OnePetro 2011, 764−767. DOI: 10.2118/144370-ms.
(27) Curtis, M. E.; Cardott, B. J.; Sondergeld, C. H.; Rai, C. S. Development of Organic Porosity in the Woodford Shale with Increasing Thermal Maturity. *Int. J. Coal Geol* **2012**, *103*, 26−31.
(28) Saidian, M.; Kuila, U.; Godinez, L. J.; Rivera, S.; Prasad, M. A Comparative Study of Porosity Measurement in MudRocks. In *Society of Exploration Geophysicists International Exposition and 84th Annual Meeting* SEG 2014, 2433−2438. DOI: 10.1190/segam2014-0426.1.
(29) Hazra, B.; Wood, D. A.; Vishal, V.; Varma, A. K.; Sakha, D.; Singh, A. K. Porosity Controls and Fractal Disposition of Organic-Rich Permian Shales Using Low-Pressure Adsorption Techniques. *Fuel* **2018**, *220*, 837−848.
(30) Yang, R.; Hu, Q.; Yi, J.; Zhang, B.; He, S.; Guo, X.; Hou, Y.; Dong, T. The Effects of Mineral Composition, TOC Content and Pore Structure on Spontaneous Imbibition in Lower Jurassic Dongyuemiao Shale Reservoirs. *Mar Pet Geol* **2019**, *109* (March), 268−278.
(31) Hazra, B.; Karacan, C. Ö.; Tiwari, D. M.; Singh, P. K.; Singh, A. K. Insights from Rock-Eval Analysis on the Influence of Sample Weight on Hydrocarbon Generation from Lower Permian Organic Matter Rich Rocks, West Bokaro Basin. *India. Mar Pet Geol* **2019**, *106* (May), 160−170.
(32) Hazra, B.; Varma, A. K.; Bandopadhyay, A. K.; Mendhe, V. A.; Singh, B. D.; Saxena, V. K.; Samad, S. K.; Mishra, D. K. Petrographic Insights of Organic Matter Conversion of Raniganj Basin Shales. *India. Int. J. Coal Geol* **2015**, *150−151*, 193−209.
(33) Hazra, B.; Singh, D. P.; Chakraborty, P.; Singh, P. K.; Sahu, S. G.; Adak, A. K. Using Rock-Eval S4Tpeak as Thermal Maturity Proxy for Shales. *Mar. Pet. Geol.* **2021**, *127*, No. 104977.
(34) Chandra, D.; Vishal, V.; Debbarma, A.; Banerjee, S.; Pradhan, S. P.; Mishra, M. K. Role of Composition and Depth on Pore Attributes of Barakar Formation Gas Shales of Ib Valley, India, Using a Combination of Low-Pressure Sorption and Image Analysis. *Energy Fuels* **2020**, *34*, 8085.
(35) Wang, C. C.; Juang, L. C.; Lee, C. K.; Hsu, T. C.; Lee, J. F.; Chao, H. P. Effects of Exchanged Surfactant Cations on the Pore Structure and Adsorption Characteristics of Montmorillonite. *J. Colloid Interface Sci.* **2004**, *280* (1), 27−35.
(36) Zhang, Y.; Shao, D.; Yan, J.; Jia, X.; Li, Y.; Yu, P.; Zhang, T. The Pore Size Distribution and Its Relationship with Shale Gas Capacity in Organic-Rich Mudstone of Wufeng-Longmaxi Formations, Sichuan Basin. *China. Journal of Natural Gas Geoscience* **2016**, *1* (3), 213−220.
(37) Furmann, A.; Mastalerz, M.; Schimmelmann, A.; Pedersen, P. K.; Bish, D. Relationships between Porosity, Organic Matter, and Mineral Matter in Mature Organic-Rich Marine Mudstones of the Belle Fourche and Second White Specks Formations in Alberta. *Canada. Mar Pet Geol* **2014**, *54*, 65−81.
(38) Liu, Y.; Hou, J. Selective Adsorption of CO2/CH4mixture on Clay-Rich Shale Using Molecular Simulations. *J. CO2 Util.* **2020**, *39*, No. 101143.
(39) Holmes, R.; Aljamaan, H.; Vishal, V.; Wilcox, J.; Kovscek, A. R. Idealized Shale Sorption Isotherm Measurements to Determine Pore Capacity, Pore Size Distribution, and Surface Area. *Energy Fuels* **2019**, *33* (2), 665−676.
(40) Labani, M. M.; Rezaee, R.; Saeedi, A.; Hinai, A. Al. Evaluation of Pore Size Spectrum of Gas Shale Reservoirs Using Low Pressure Nitrogen Adsorption, Gas Expansion and Mercury Porosimetry: A Case Study from the Perth and Canning Basins, Western Australia. *J. Pet Sci. Eng.* **2013**, *112*, 7−16.
(41) Chen, Y.; Wei, L.; Mastalerz, M.; Schimmelmann, A. The Effect of Analytical Particle Size on Gas Adsorption Porosimetry of Shale. *Int. J. Coal Geol* **2015**, *138*, 103−112.
(42) Li, T.; Tian, H.; Chen, J.; Cheng, L. Application of Low-Pressure Gas Adsorption to the Characterization of Pore Size Distribution of Shales: An Example from Southeastern Chongqing Area. *China. Journal of Natural Gas Geoscience* **2016**, *1* (3), 221−230.
(43) Han, H.; Cao, Y.; Chen, S. J.; Lu, J. G.; Huang, C. X.; Zhu, H. H.; Zhan, P.; Gao, Y. Influence of Particle Size on Gas-Adsorption Experiments of Shales: An Example from a Longmaxi Shale Sample from the Sichuan Basin, China. *Fuel* **2016**, *186*, 750−757.
(44) Mastalerz, M.; Hampton, L. B.; Drobniak, A.; Loope, H. Significance of Analytical Particle Size in Low-Pressure N2 and CO2 Adsorption of Coal and Shale. *Int. J. Coal Geol* **2017**, *178*, 122−131.
(45) Sang, G.; Liu, S.; Zhang, R.; Elsworth, D.; He, L. Nanopore Characterization of Mine Roof Shales by SANS, Nitrogen Adsorption, and Mercury Intrusion: Impact on Water Adsorption/Retention Behavior. *Int. J. Coal Geol* **2018**, *200* (July), 173−185.
(46) Radlinski, A. P.; Mastalerz, M.; Hinde, A. L.; Hainbuchner, M.; Rauch, H.; Baron, M.; Lin, J. S.; Fan, L.; Thiyagarajan, P. Application of SAXS and SANS in Evaluation of Porosity, Pore Size Distribution and Surface Area of Coal. *Int. J. Coal Geol* **2004**, *59* (3−4), 245−271.
(47) Mastalerz, M.; He, L.; Melnichenko, Y. B.; Rupp, J. A. Porosity of Coal and Shale: Insights from Gas Adsorption and SANS/USANS Techniques. *Energy Fuels* **2012**, *26* (8), 5109−5120.
(48) Bahadur, J.; Melnichenko, Y. B.; Mastalerz, M.; Furmann, A.; Clarkson, C. R. Hierarchical Pore Morphology of Cretaceous Shale: A Small-Angle Neutron Scattering and Ultrasmall-Angle Neutron Scattering Study. *Energy Fuels* **2014**, *28* (10), 6336−6344.
(49) Bahadur, J.; Melnichenko, Y. B.; He, L.; Contescu, C. I.; Gallego, N. C.; Carmichael, J. R. SANS Investigations of CO2 Adsorption in Microporous Carbon. *Carbon N Y* **2015**, *95*, 535−544.
(50) Stefanopoulos, K. L.; Youngs, T. G. A.; Sakurovs, R.; Ruppert, L. F.; Bahadur, J.; Melnichenko, Y. B. Neutron Scattering Measurements

of Carbon Dioxide Adsorption in Pores within the Marcellus Shale: Implications for Sequestration. *Environ. Sci. Technol.* **2017**, *51* (11), 6515−6521.
(51) Okolo, G. N.; Everson, R. C.; Neomagus, H. W. J. P.; Sakurovs, R.; Grigore, M.; Bunt, J. R. The Carbon Dioxide, Methane and Nitrogen High-Pressure Sorption Properties of South African Bituminous Coals. *Int. J. Coal Geol.* **2019**, *209*, 40−53.
(52) Chandra, D.; Bakshi, T.; Bahadur, J.; Hazra, B.; Vishal, V.; Kumar, S.; Sen, D.; Singh, T. N. Pore Morphology in Thermally Treated Shales and Its Implication on CO2 Storage Applications: A Gas Sorption, SEM, and Small-Angle Scattering Study. *Fuel* **2023**, *331* (P2), No. 125877.
(53) Rezaeyan, A.; Pipich, V.; Busch, A. MATSAS: A Small-Angle Scattering Computing Tool for Porous Systems. *J. Appl. Crystallogr.* **2021**, *54*, 697−706.
(54) Bhapkar, P. V.; Pradhan, S. P.; Chandra, D.; Hazra, B.; Vishal, V. Systematic Pore Characterization of Sub-Bituminous Coal from Sohagpur Coalfield, Central India Using Gas Adsorption Coupled with X-Ray Scattering and High-Resolution Imaging. *Energy Fuels* **2023**, *37* (13), 9297−9308.
(55) Hazra, B.; Chandra, D.; Singh, A. K.; Varma, A. K.; Mani, D.; Singh, P. K.; Boral, P.; Buragohain, J. Comparative Pore Structural Attributes and Fractal Dimensions of Lower Permian Organic-Matter-Bearing Sediments of Two Indian Basins: Inferences from Nitrogen Gas Adsorption. *Energy Sources, Part A: Recovery, Utilization and Environmental Effects* **2019**, *41* (24), 2975−2988.
(56) Mandelbrot, B. B.; Passoja, D. E.; Paullay, A. J. Fractal Character of Fracture Surfaces of Metals. *Nature* **1984**, *308* (5961), 721−722.
(57) Chalmers, G. R.; Bustin, R. M.; Power, I. M. Characterization of Gas Shale Pore Systems by Porosimetry, Pycnometry, Surface area, And field Emission Scanning Electron Microscopy/ Transmission Electron Microscopy Image Analyses: Examples from the Barnett, Woodford, Haynesville, Marcellus, And Doig Units. *Am. Assoc Pet Geol Bull.* **2012**, *96* (6), 1099−1119.
(58) Bu, H.; Ju, Y.; Tan, J.; Wang, G.; Li, X. Fractal Characteristics of Pores in Non-Marine Shales from the Huainan Coalfield, Eastern China. *J. Nat. Gas Sci. Eng.* **2015**, *24*, 166−177.
(59) Zhang, K.; Cheng, Y.; Jin, K.; Guo, H.; Liu, Q.; Dong, J.; Li, W. Effects of Supercritical CO2 Fluids on Pore Morphology of Coal: Implications for CO2 Geological Sequestration. *Energy Fuels* **2017**, *31* (5), 4731−4741.
(60) Bai, F.; Sun, Y.; Liu, Y.; Guo, M. Evaluation of the Porous Structure of Huadian Oil Shale during Pyrolysis Using Multiple Approaches. *Fuel* **2017**, *187*, 1−8.
(61) Holmes, R.; Rupp, E. C.; Vishal, V.; Wilcox, J. Selection of Shale Preparation Protocol and Outgas Procedures for Applications in Low-Pressure Analysis. *Energy Fuels* **2017**, *31* (9), 9043−9051.
(62) Hazra, B.; Wood, D. A.; Vishal, V.; Singh, A. K. Pore Characteristics of Distinct Thermally Mature Shales: Influence of Particle Size on Low-Pressure CO2 and N2 Adsorption. *Energy Fuels* **2018**, *32* (8), 8175−8186.
(63) Chandra, D.; Vishal, V.; Bahadur, J.; Sen, D. A Novel Approach to Identify Accessible and Inaccessible Pores in Gas Shales Using Combined Low-Pressure Sorption and SAXS/SANS Analysis. *Int. J. Coal Geol.* **2020**, *228*, No. 103556.
(64) Zhang, S.; Tang, S.; Tang, D.; Huang, W.; Pan, Z. Determining Fractal Dimensions of Coal Pores by FHH Model: Problems and Effects. *J. Nat. Gas Sci. Eng.* **2014**, *21*, 929−939.
(65) Yu, S.; Bo, J.; Fengli, L.; Jiegang, L. Structure and Fractal Characteristic of Micro- and Meso-Pores in Low, Middle-Rank Tectonic Deformed Coals by CO2 and N2 Adsorption. *Microporous Mesoporous Mater.* **2017**, *253*, 191−202.
(66) Liu, K.; Ostadhassan, M.; Jang, H. W.; Zakharova, N. V.; Shokouhimehr, M. Comparison of Fractal Dimensions from Nitrogen Adsorption Data in Shale: Via Different Models. *RSC Adv.* **2021**, *11* (4), 2298−2306.
(67) Wood, D. A. Estimating Organic-Rich Shale Fractal Dimensions from Gas Adsorption Isotherms: Combining Different Methods Leads to More Reliable Values and Insight. *Natural Resources Research* **2021**, *30* (5), 3551−3574.
(68) Yang, Y.; Zhang, J.; Xu, L.; Li, P.; Liu, Y.; Dang, W. Pore Structure and Fractal Characteristics of Deep Shale: A Case Study from Permian Shanxi Formation Shale, from the Ordos Basin. *ACS Omega* **2022**, *7* (11), 9229−9243.
(69) Mukhopadhyay, G.; Mukhopadhyay, S. K.; Roychowdhury, M.; Parui, P. K. Stratigraphic Correlation between Different Gondwana Basins of India. *Journal of the Geological Society of India* **2010**, *76* (3), 251−266.
(70) Singh, K. J.; Saxena, A.; Goswami, S. Palaeobiodiversity of the Lower Gondwana Rocks in the Korba Coalfield, Chhattisgarh, India and Observations on the Genus Gangamopteris McCoy. *J. Palaeosciences* **2012**, *61* (1−2), 145−163.
(71) Tewari, R. C.; Hota, R. N.; Maejima, W. Fluvial Architecture of Early Permian Barakar Rocks of Korba Gondwana Basin. *Eastern-Central India. J. Asian Earth Sci.* **2012**, *52*, 43−52.
(72) Varma, A. K.; Hazra, B.; Samad, S. K.; Panda, S.; Mendhe, V. A. Methane Sorption Dynamics and Hydrocarbon Generation of Shale Samples from West Bokaro and Raniganj Basins. *India. J. Nat. Gas Sci. Eng.* **2014**, *21*, 1138−1147.
(73) *Geological Survey of India*, 2005, District Resource MAP of Korba, Chhattisgarh. https://employee.gsi.gov.in/cs/groups/public/documents/document/b3zp/otex/~edisp/dcport1gsigovi911919.jpg.
(74) Hazra, B.; Dutta, S.; Kumar, S. TOC Calculation of Organic Matter Rich Sediments Using Rock-Eval Pyrolysis: Critical Consideration and Insights. *Int. J. Coal Geol* **2017**, *169*, 106−115.
(75) Hazra, B.; Karacan, C. Ö.; Tiwari, D. M.; Singh, P. K.; Singh, A. K. Insights from Rock-Eval Analysis on the Influence of Sample Weight on Hydrocarbon Generation from Lower Permian Organic Matter Rich Rocks, West Bokaro Basin. *India. Mar Pet Geol* **2019**, *106*, 160−170.
(76) Wei, M.; Xiong, Y.; Zhang, L.; Li, J.; Peng, P. The Effect of Sample Particle Size on the Determination of Pore Structure Parameters in Shales. *Int. J. Coal Geol* **2016**, *163*, 177−185.
(77) Yang, C.; Xiong, Y.; Zhang, J. A Comprehensive Re-Understanding of the OM-Hosted Nanopores in the Marine Wufeng−Longmaxi Shale Formation in South China by Organic Petrology, Gas Adsorption, and X-Ray Diffraction Studies. *Int. J. Coal Geol.* **2020**, *218*, No. 103362.
(78) Singh, D. P.; Chandra, D.; Vishal, V.; Hazra, B.; Sarkar, P. Impact of Degassing Time and Temperature on the Estimation of Pore Attributes in Shale. *Energy Fuels* **2021**, *35*, 15628 DOI: 10.1021/acs.energyfuels.1c02201.
(79) Neimark, A. V.; Lin, Y.; Ravikovitch, P. I.; Thommes, M. Quenched Solid Density Functional Theory and Pore Size Analysis of Micro-Mesoporous Carbons. *Carbon N Y* **2009**, *47* (7), 1617−1628.
(80) Landers, J.; Gor, G. Y.; Neimark, A. V. Density Functional Theory Methods for Characterization of Porous Materials. *Colloids Surf. A Physicochem Eng. Asp* **2013**, *437*, 3−32.
(81) Thommes, M.; Kaneko, K.; Neimark, A. V.; Olivier, J. P.; Rodriguez-Reinoso, F.; Rouquerol, J.; Sing, K. S. W. Physisorption of Gases, with Special Reference to the Evaluation of Surface Area and Pore Size Distribution (IUPAC Technical Report). *Pure Appl. Chem.* **2015**, *87* (9−10), 1051−1069.
(82) Cychosz, K. A.; Thommes, M. Progress in the Physisorption Characterization of Nanoporous Gas Storage Materials. *Engineering*. Elsevier Ltd, **2018**, *1*, 559 566 DOI: .
(83) Groen, J. C.; Peffer, L. A. A.; Pérez-Ramírez, J. Pore Size Determination in Modified Micro- and Mesoporous Materials. Pitfalls and Limitations in Gas Adsorption Data Analysis. *Microporous Mesoporous Mater.* **2003**, *60* (1−3), 1−17.
(84) Wang, M.; Xue, H.; Tian, S.; Wilkins, R. W. T.; Wang, Z. Fractal Characteristics of Upper Cretaceous Lacustrine Shale from the Songliao Basin. *NE China. Mar Pet Geol* **2015**, *67*, 144−153.
(85) Liu, X.; Xiong, J.; Liang, L. Investigation of Pore Structure and Fractal Characteristics of Organic-Rich Yanchang Formation Shale in Central China by Nitrogen Adsorption/Desorption Analysis. *J. Nat. Gas Sci. Eng.* **2015**, *22*, 62−72.

(86) Mishra, S.; Mendhe, V. A.; Varma, A. K.; Kamble, A. D.; Sharma, S.; Bannerjee, M.; Kalpana, M. S. Influence of Organic and Inorganic Content on Fractal Dimensions of Barakar and Barren Measures Shale Gas Reservoirs of Raniganj Basin. *India. J. Nat. Gas Sci. Eng.* **2018**, *49*, 393−409.
(87) Ismail, I. M. K.; Pfeifer, P. Fractal Analysis and Surface Roughness of Nonporous Carbon Fibers and Carbon Blacks. *Langmuir* **1994**, *10*, 1532−1538.
(88) Chandra, D.; Vishal, V. A Comparative Analysis of Pore Attributes of Sub-Bituminous Gondwana Coal from the Damodar and Wardha Valleys: Implication for Enhanced Coalbed Methane Recovery. *Energy Fuels* **2022**, *36*, 6187.
(89) Feng, G.; Li, W.; Zhu, Y.; Wang, Y.; Song, Y.; Zheng, S.; Shang, F. Scale-Dependent Fractal Properties and Geological Factors for the Pore Structure in Shale: Insights from Field Emission Scanning Electron Microscopy and Fluid Intrusion. *Energy Fuels* **2023**, *37* (21), 16519−16535.
(90) Ma, X.; Guo, S.; Shi, D.; Zhou, Z.; Liu, G. Investigation of Pore Structure and Fractal Characteristics of Marine-Continental Transitional Shales from Longtan Formation Using MICP, Gas Adsorption, and NMR (Guizhou, China). *Mar Pet Geol* **2019**, *107*, 555−571.
(91) Li, Z.; Zhang, J.; Mo, X.; Tong, Z.; Wang, X.; Wang, D.; Su, Z.; Tang, X.; Gong, D. Characterization of an Angstrom-Scale Pore Structure in Organic-Rich Shales by Using Low-Pressure CO2Adsorption and Multifractal Theory and Its Role in CH4/CO2Gas Storage. *Energy Fuels* **2022**, *36* (19), 12085−12103.

https://doi.org/10.1021/acs.energyfuels.3c03374
Energy Fuels 2024, 38, 3833−3847